2006

# Microtexture and microstructure evolution during processing of pure aluminum by repetitive EACP

Zhilyaev, A. P.

Elsevier

ELSEVIER

Materials Science and Engineering A 429 (2006) 137–148

MATERIALS SCIENCE & ENGINEERING A

www.elsevier.com/locate/msea

# Microtexture and microstructure evolution during processing of pure aluminum by repetitive ECAP

A.P. Zhilyaev [a,1], D.L. Swisher [a], K. Oh-ishi [a,2], T.G. Langdon [b], T.R. McNelley [a,*]

[a] *Department of Mechanical & Astronautical Engineering, Naval Postgraduate School, 700 Dyer Road, Monterey, CA 93943-5146, USA*

[b] *Departments of Aerospace & Mechanical Engineering and Materials Science, University of Southern California, Los Angeles, CA 90089-1453, USA*

Received 1 March 2006; received in revised form 2 May 2006; accepted 3 May 2006

**Abstract**

Microtexture and microstructure evolution during repetitive equal-channel angular pressing (ECAP) of pure aluminum through a 90° die was evaluated by orientation imaging microscopy (OIM) and transmission electron microscopy (TEM). Billet distortion appears to conform to the idealized ECAP model. After the initial pass, the textures were inhomogeneous but one or more shear-texture components and long-range lattice rotations were apparent. Following repetitive ECAP, the textures became more homogeneous but still included either two or three distinct shear-texture orientations. The OIM and TEM data revealed meso-scale deformation bands that were inclined at about 26° to the axis of the as-pressed samples and that involved alternation of lattice orientations between distinct shear-texture orientations. The band interfaces were of high disorientation (40–62.8°) and were distinct boundaries in TEM. The evolution of the band structures during repetitive ECAP accounts for an increasing population of high-angle boundaries in repetitively processed materials.


*Keywords:* Aluminum; Equal-channel angular pressing (ECAP); Texture; Orientation imaging microscopy (OIM); Deformation Banding; Grain boundaries

## 1. Introduction

The homogenization and refinement of microstructure by deformation processing is beneficial to the mechanical properties of engineering materials. Highly refined grains contribute to ambient strength and may lead also to low-temperature superplasticity [1,2]. Many studies have shown that ultra-fine grain sizes, in the sub-micrometer or even nanometer range, may be achieved by imposing extremely large plastic strains through processing by severe plastic deformation (SPD) [3–6]. Equal-channel angular pressing (ECAP) has been widely studied as a promising SPD method. However, the dependence of texture development on ECAP process parameters (e.g., die geometry) and material properties (e.g., stacking fault energy) [7–10] has not been clarified and there is little information on the mechanisms by which the ultra-fine grains and high-angle boundaries evolve in the deformation-induced microstructures.

In an idealized description of ECAP, deformation takes place by simple shear confined to a narrow zone at the plane of intersection of the die channels, as illustrated in Fig. 1. In this schematic, a billet is pressed downward in the die entrance channel in the $-y$-direction and exits the die in the $+x$-direction through the die exit channel. The theoretical shear plane is then the plane of the die channel intersection (the trace of this plane is indicated by the dotted line), and the shear direction (SD; indicated by the half-arrows) is aligned with the bisector of the axes of the die entrance and the die exit channels. The shear textures for the torsional deformation of face-centered cubic metals have been described by Jonas and co-workers [11,12]. Thus, aluminum is expected to exhibit corresponding shear textures following ECAP at room temperature but in relation to axes coupled with the theoretical shear plane/SD of the die, i.e., the $x'$–$y'$–$z'$-axes in Fig. 1. Friction between the billet and the die wall may also complicate an analysis of the ECAP textures.

The experimental ECAP textures generally follow this expectation, as shown in a study of an aluminum single crystal [13] that was specially oriented in the entrance channel of the ECAP die.

* Corresponding author. Tel.: +1 831 656 2216; fax: +1 831 656 2238.
*E-mail address:* TMcNelley@nps.edu (T.R. McNelley).

[1] On leave from Institute for Metals Superplasticity Problems, Russian Academy of Science, 450001 39 Khalturina Str., Ufa, Russia.

[2] Present address: National Institute for Materials Science, 1-2-1 Sengen, Tsukuba 305-0047, Japan.

0921-5093/$ – see front matter © 2006 Elsevier B.V. All rights reserved.
doi:10.1016/j.msea.2006.05.009

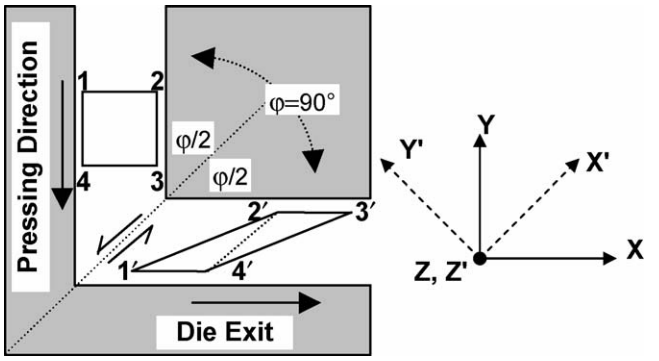


Fig. 1. A schematic of an ECAP die having a 90° angle between the die channels.

For ECAP of polycrystalline aluminum, experimental [9,14,15] and model [16] shear textures generally exhibit various rotations about the flow plane normal (FPN; the $z$-axis in Fig. 1). For example, Tóth et al. [17] concluded that ECAP of oxygen-free copper gave a simple shear texture but with deviations of 20° from the ideal orientations for repetitively-pressed samples. These deviations were simulated by a 'texture correction' method based on the Taylor and self-consistent approaches. Similar texture orientations were also reported [18] in ECAP of aluminum although the texture was described in the billet axis system, i.e., the $x$–$y$–$z$ system in Fig. 1, wherein the SD was assumed to align with $x$-axis and the shear plane coincided with the $y$-plane. A C-type component [11], $\{0\,0\,1\}\langle 1\,1\,0\rangle$, where the notation refers to $\{$plane parallel to the shear plane$\}\langle$direction parallel to the SD$\rangle$, and a distinct orientation along the B-fiber, $\{1\,1\,2\}\langle 1\,1\,0\rangle$, were reported. However, in repetitively-pressed material these, components were rotated by ∼15–20° about the FPN in these axes and no data were reported for the initial pass. Texture modeling by a fully-constrained Taylor approach predicted this rotation when an experimentally measured deformation history was used as an input for the calculations. From the foregoing, it is apparent there is disagreement in the ECAP literature regarding the choice of axes for specifying textures and describing strains. This leads to complications in correlation of textures and microstructures.

Typically, ECAP is carried out at low homologous temperatures and it has been shown that the resulting deformation-induced microstructures evolve in a manner similar to those produced by cold-working [19]. Recent overviews [20,21] have described cold-worked microstructures and provided catalogs of various features that evolve during cold-rolling. The processes of grain subdivision include the formation and evolution of lamellar boundaries (LBs), microbands (MBs) and dense dislocation walls (DDWs) as well as subgrains and cellular substructures. The LBs, MBs and DDWs elongate as the prior grains deform and the LBs and MBs become band-like features with high disorientation boundaries that eventually align with the rolling direction. These features generally separate regions within prior grains that have experienced lattice rotation in opposite senses away from the original grain orientation. Deformation banding (DB) is also a process of grain subdivision wherein the lattice rotates in different senses in adjacent regions of the prior grains but towards symmetrically-related end orientations in the texture [22].[3] Superplastic Al–Cu–Zr and Al–Ca–Zn alloys exhibit DB formation with distinct single-component cold-rolling textures, and high-angle boundaries form from the interfaces between adjacent DBs during subsequent elevated temperature deformation [23,24]. Processes of grain subdivision and high-angle boundary formation in ECAP materials have been cited recently [20,21], analogous to processes in rolled materials [25,26]. The differences in the relative populations of low- and high-angle boundaries reflect, in part, different experimental techniques. Most investigations have used transmission electron microscopy (TEM) and there have been few meso-scale studies of texture and DB in association with ECAP [20]. The present report documents the results of such an investigation of microtexture, microstructure and grain boundary statistics during the repetitive ECAP of pure aluminum. The OIM data reveal distinct shear-texture components where well-defined DBs form in repetitively-pressed materials and the TEM data show that the band–band interfaces are well-defined boundaries. The results lead to a proposed mechanism for the development of high-angle boundaries where this mechanism is consistent with proposals in the literature [21].

## 2. Experimental procedures

Pure (99.99%) aluminum was rolled into a plate at room temperature and cut to provide billets with dimensions of 25 mm × 25 mm × 150 mm. These billets were swaged at room temperature to rods 10 mm in diameter and the rods were then cut into lengths of ∼60 mm. Prior to ECAP, the billets were given an annealing treatment leading to an initial recrystallized grain size of ∼1 mm. Investigations by X-ray revealed an essentially random texture in the annealed samples although neutron diffraction gave some evidence for a $\langle 1\,1\,1\rangle$ fiber texture [27]. Samples were pressed following the definitions of routes A, $B_C$ and C for repetitive pressing operations through a 90° die using a plunger speed of 19 mm $s^{-1}$. The die had a 20° relief angle at the outer corner of the die channel intersection but it is known that this will not significantly affect the pressed microstructures [28].

Details of the sample preparation for TEM and orientation imaging microscopy (OIM) were given previously [9] and the observation procedures followed conventional practice [29]. Special care was taken to determine the orientations and senses of the billet axes in the TEM for each 3 mm disk. The TEM images and convergent beam electron diffraction (CBED) patterns were captured using a Gatan[4] DualView300 digital camera

[3] Deformation banding in this report follows the earlier formal definition given by Kuhlmann-Wilsdorf [22] where it was noted that some "constraints limit the local operation of intersecting slip systems to only two or perhaps three, and apparently never permit four or five. Consequently, all polycrystal deformation and multiple glide in single crystals causes different lattice reorientations in neighboring volume elements because of the different selection of locally operating slip systems. The resulting lattice misorientations appear as deformation bands".

[4] Gatan Inc., Pleasanton, CA.

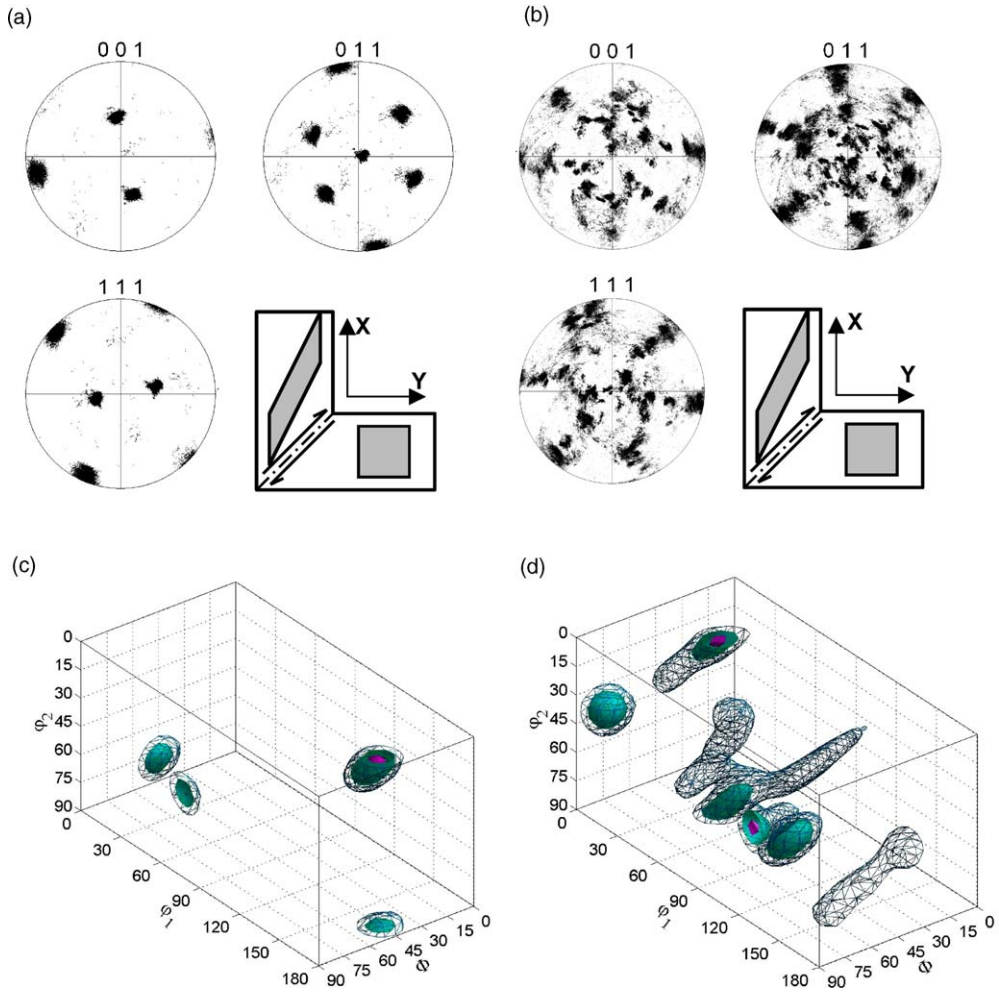


Fig. 2. Pole figures in ECAP aluminum after one pass: (a) 100 μm × 100 μm region; (b) 3750 μm × 10 μm region. Corresponding 3D representation of ODFs for one pass ECAP aluminum; (c) 100 μm × 100 μm region (maximum intensity is 154.4 × random); (d) 3750 μm × 10 μm region (maximum intensity is 22.8 × random). Surfaces: 1/4, 1/2 and 3/4 of maximum intensity.

installed on a TOPCON[5] EM-002B microscope equipped and controlled by Digital Micrograph (Gatan Inc.) software.

In order to assist in interpretation of the experimental textures, a simple shear texture corresponding to a single ECAP pass was computed using the visco-plastic self-consistent (VPSC) code [16,30] with a random input texture. The VPSC code assumes that a polycrystalline material may be represented by means of weighted orientations representing the initial texture. The VPSC output was used with the OIM software to represent the texture data as pole figures, and orientation distribution functions (ODFs).

The ODFs for both experimental and VPSC textures were then calculated assuming monoclinic symmetry for simple shear in the $x$–$y$–$z$ coordinate system illustrated in Fig. 1. This coordinate system was chosen so that the $x$-direction coincides with the die exit direction. An as-pressed ECAP billet exhibits monoclinic symmetry with the FPN as the two-fold axis and this symmetry requires that the sense and the orientation of the axes be preserved for each sample in any representation of the orientation data. The axis system depicted in Fig. 1 facilitates representation of the fundamental zone of Euler space in that the initial Euler rotation, $\varphi_1$, about $z$ must be $0^\circ \leq \varphi_1 \leq 180^\circ$ [29] for a face centered cubic metal. In this case, differences between experimental and ideal textures that involve small rotations about the FPN will be reflected in small displacements along only $\varphi_1$. Here, the calculated ODFs are represented in 3D views by isosurfaces of 1/4, 1/2 and 3/4 of the maximum intensity in the fundamental zone of Euler space.

## 3. Experimental results

### 3.1. OIM analysis of microtexture, microstructure and GB misorientations in aluminum processed by ECAP

#### 3.1.1. One ECAP pass

In previous reports [9,31], TEM data revealed a fine subgrain structure in the pure aluminum but OIM results showed inhomogeneous microtextures and microstructures after a single ECAP pass. A representative set of pole figures from a region having a size of 100 μm × 100 μm and located at the center of the flow plane is included in Fig. 2(a). These data reveal a distinct A-type

[5] TOPCON America Corp., Paramus, NJ.

shear-texture component, $(1\,1\,\bar{1})[1\,1\,2]$, that is aligned with the plane of the die channel intersection in Fig. 1. Thus, the apparent shear plane, $\{1\,1\,1\}$, is nearly parallel to the plane of the die channel intersection while the SD, $\langle 1\,1\,2\rangle$, is nearly parallel to the bisector of the die angle. This coincides with the idealized description of ECAP wherein the SD is expected to align and bisect the die channel angle so that it lies in a direction located at 45° counterclockwise about the $z$-axis from the billet axis. Fig. 2(b) shows a set of pole figures obtained by scanning with the same step size as in Fig. 2(a) but covering a larger area of 3750 μm × 10 μm with the long axis of the scan aligned with the diameter of the as-pressed billet. The length of this scan is ∼38% of the billet diameter. This is also a shear texture, as shown by comparison with results reported by Jonas et al. [11,12], and again the SD is nearly aligned to bisect the die channel angle. The distribution of orientations in Fig. 2(b) is consistent with the presence of an A-type shear-texture fiber, $\{1\,1\,\bar{1}\}\langle uvw\rangle$, and a B-fiber component, $\{1\,\bar{1}\,\bar{2}\}\langle\bar{1}\,\bar{1}\,0\rangle$.

Fig. 2(c) shows the 3D ODF corresponding to the pole figures of Fig. 2(a). The A-type shear component has a peak intensity of 115.4 although the peak location is displaced about 10° from the expected location in the axes in Fig. 1. The peak intensities for the larger area scan, shown in Fig. 2(d), are almost an order of magnitude smaller. Nevertheless, a variant of the same A-type fiber is still present and additional orientations form clusters that are located near $\{1\,1\,1\}\langle 1\,1\,2\rangle$. Additionally, a B-fiber component, $\{1\,\bar{1}\,\bar{2}\}\langle\bar{1}\,\bar{1}\,0\rangle$, is apparent in the texture.

Fig. 3 shows an OIM inverse pole figure map for a 100 μm × 100 μm region and superimposed is a linear traverse for calculation of the point-to-origin lattice disorientations. The near-uniform color indicates that this area corresponds to a single zone axis although gradations in shading signify the presence of a substructure with boundaries of disorientation below 15°. Indeed, the point-to-origin disorientation traverse reveals the presence of long-range lattice rotations involving a gradual accumulation of 3–5° of disorientation over 100 μm. This may account for the orientation scatter in the textures.

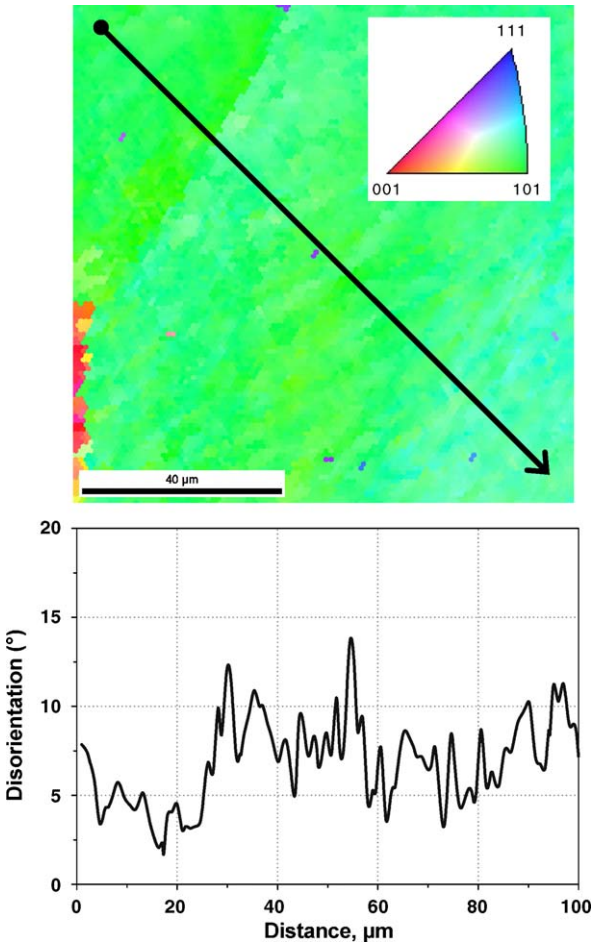


Fig. 3. Long-range lattice rotations are apparent in a substructure at the orientation resolution of OIM.

### 3.1.2. Four ECAP passes

The OIM results for pure aluminum after four ECAP passes are given in Fig. 4. These results include point-to-origin disorientation plots, color-highlighted image quality (IQ) maps and pole figures for each of the three repetitive pressing routes (A, $B_C$ and C). The point-to-origin disorientation plots in Fig. 4(a) correspond to the traverses indicated on the IQ maps in Fig. 4(b). Lattice orientations and their locations are stored during OIM scanning; thus, the IQ maps in Fig. 4(b) are highlighted to identify the distributions of lattice orientations in the microstructures using a color-coding corresponding to the pole figures of Fig. 4(c).

The data of Fig. 4 show that DBs develop for all three processing routes. The DBs involve alternating lattice orientations separated by large disorientation (≥40°) boundaries. The distinct orientation change upon crossing the DB interfaces is apparent in the point-to-origin traverses by the abrupt changes in disorientation in Fig. 4(a) and in color in Fig. 4(b). The DBs vary in width from approximately 5–25 μm. In routes A and $B_C$, the interfaces between adjacent bands are inclined at an angle of ∼26° to the $x$-axis. The band structure in material processed by route C is more complex and there are at least three distinct orientations in the microstructure. In a previous report, TEM and OIM data documented the presence of a refined (sub)grain structure with a mean linear intercept size of ∼1.2 μm [9]. Furthermore, a more recent investigation has shown that the fraction of high-angle boundaries increases significantly from the first to the fourth pressing operation but there are no significant differences in the relative fractions of high-angle boundaries in the disorientation distributions following four ECAP passes by routes A, $B_C$ or C, at least within the error associated with the data collection method [32]. The textures developed after four pressing operations remain inhomogeneous when examined at a scale less than ∼10% of the sample diameter. The meso-scale textures for all routes contain A- and B-type fiber shear-texture orientations in addition to C-type orientations. A comparison of the 011 pole figures for materials after four ECAP passes by routes A and $B_C$ reveals the same texture orientation observed after the initial ECAP pass as shown in Fig. 2(a).

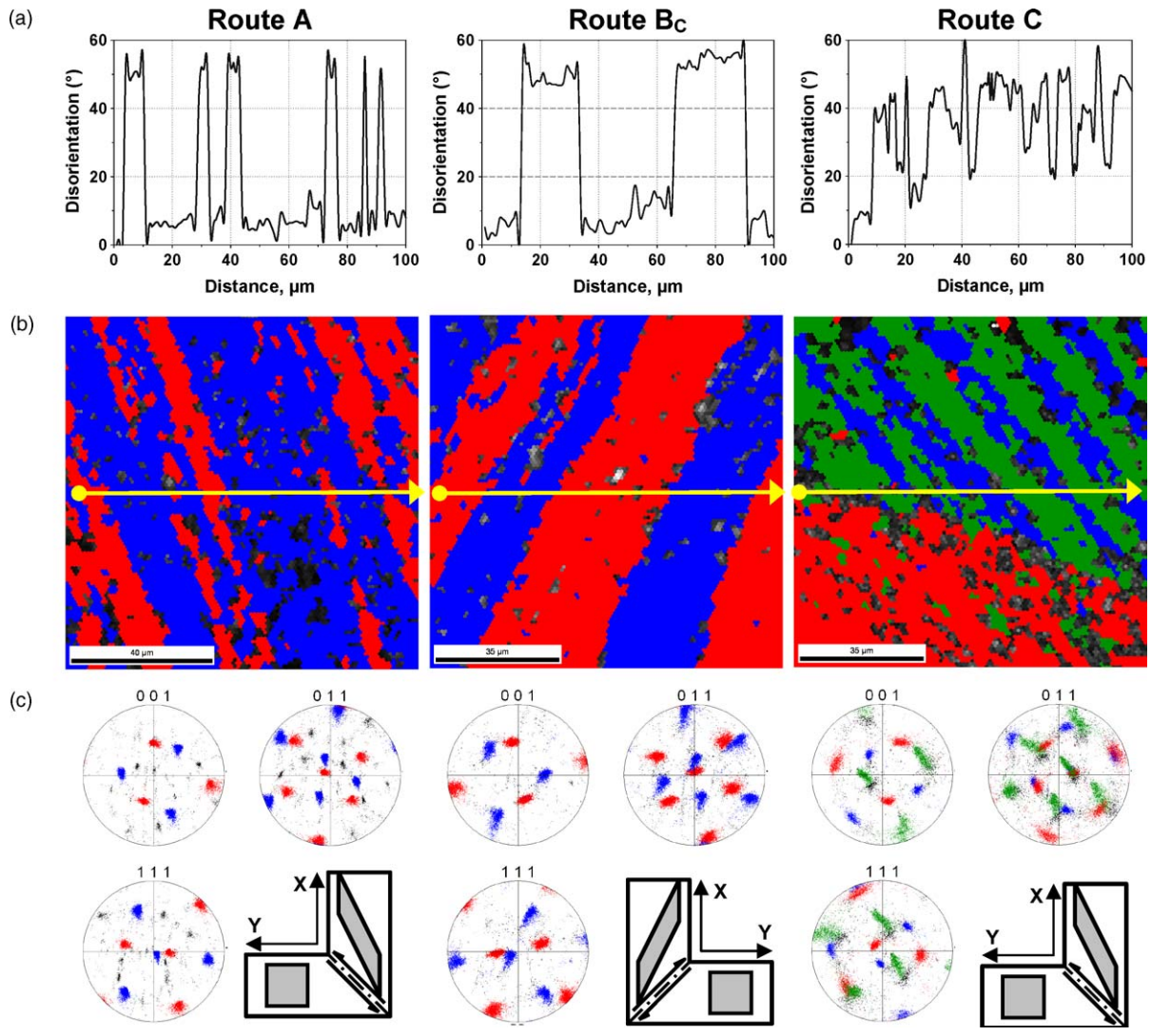


Fig. 4. Deformation bands are evident in the aluminum after four ECAP passes by routes A, $B_C$ and C; point-to-origin disorientations (a), highlighted image quality maps (b), and corresponding pole figures (c). The coordinate axis systems for these data are defined in Fig. 1.

### 3.1.3. Twelve ECAP passes

The data for material processed through 12 ECAP passes are summarized in Fig. 5. The point-to-origin plots indicate a short-range variation in grain orientations and thus a smaller separation distance between high-angle boundaries when compared to the data following four passes. This is also apparent in the IQ maps. Measurements by TEM and OIM show these structures comprise refined (sub)grains having a size of ~1.0 μm for all routes [9]. The elongated bands apparent after 4 passes are no longer distinct after 12 passes. All of these materials exhibit shear textures as shown in Fig. 5(c) but the distribution of orientations differs according to the specific processing route. It is noteworthy also that these shear textures are now homogeneous at the scale of the maps in Fig. 5(b) and also the textures include a higher proportion of random orientations after 12 passes.

Fig. 6 provides 3D ODFs for material repetitively pressed by route $B_C$. After four passes there are two distinct orientations in the texture as shown in Fig. 6(a): one of these is the C-component and the other is an orientation near the intersection of one branch of the A- and B-fibers. In material processed by 12 passes, the C-component is no longer present but clusters of orientations appear at the locations of both of the symmetrically equivalent A/B-fiber intersections.

### 3.2. TEM investigation of microstructure and microtexture in aluminum processed by route $B_C$

Fig. 7 shows a montage of bright field TEM images for material repetitively processed through four passes by route $B_C$. Mean linear intercept measurements indicate a (sub)grain size of ~1.2 μm in this region which extends by ~30 μm along the *y*-axis. The Euler angles for the orientations of all (sub)grains in this region were determined by CBED analysis and the stereographic projections in Fig. 7 show corresponding 002 orientations in the billet axis system for selected orientation measurements. Disorientations were determined for all

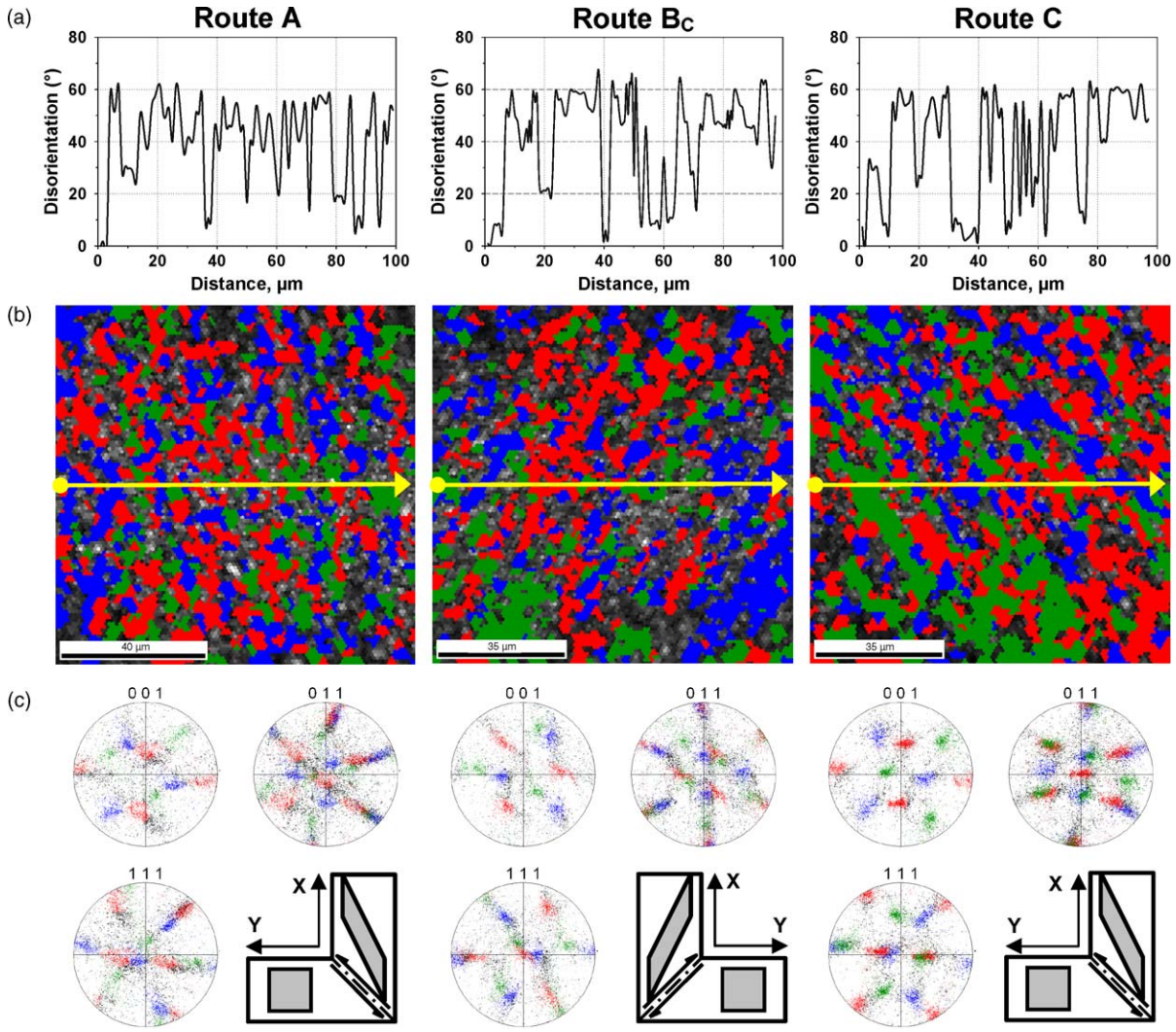


Fig. 5. Deformation bands have evolved in the aluminum after 12 ECAP passes by routes A, $B_C$ and C; point-to-origin disorientations (a), highlighted image quality maps (b), and corresponding pole figures (c). The coordinate axis systems for these data are defined in Fig. 1.

apparent boundaries in this region and the lighter or heavier superimposed lines in Fig. 7 indicate boundaries having disorientations of 15–40 or 40–62.8°, respectively. In this region the TEM data also reveal a DB structure. The high-angle (40–62.8°) boundaries delineate bands that are inclined to the *x*-axis and have alternating lattice orientations. The alternating orientations in the TEM data are close to the shear-texture components obtained by OIM. A similar TEM analysis was conducted on material processed through 12 ECAP passes by route $B_C$ and the results are shown in Fig. 8. For this condition, mean linear intercept measurements indicate a (sub)grain size of ~1.0 μm. The disorientation data from the CBED analysis is consistent with a short-range variation of orientation in the structure and the development of a higher fraction of high-angle boundaries after 12 repetitive pressing operations. It should be noted that a significant population of 10–15° boundaries (indicated by the dashed lines in Fig. 8) appear in the material after 12 ECAP passes by route $B_C$. A pattern of alternation in lattice orientations is not apparent in the 002 stereographic projections for this region although there is a tendency for the grains to be slightly elongated and aligned with the direction of the last shearing operation.

### *3.3. Grain boundary statistics in aluminum processed by ECAP*

Fig. 9 represents the distributions of the grain boundary disorientation angles and Table 1 gives the corresponding fractions of high-angle boundaries (HAB) for aluminum subjected to 1, 4 and 12 passes using routes A, $B_C$ and C. For one pass, a line scan of 3750 μm × 10 μm was used to evaluate the fraction of high-angle boundaries. For the scanned area, the material processed through one pass exhibited the lowest population of HABs. All correlated distributions in Fig. 9 are bimodal, with a low-angle peak at <10° and a second peak at approximately 54°. In Fig. 9(a, c and e), and in Table 1, route C appears to give a higher fraction of HABs after 4 passes while route $B_C$ produces the highest fraction of HABs after 12 passes. However, the differences for

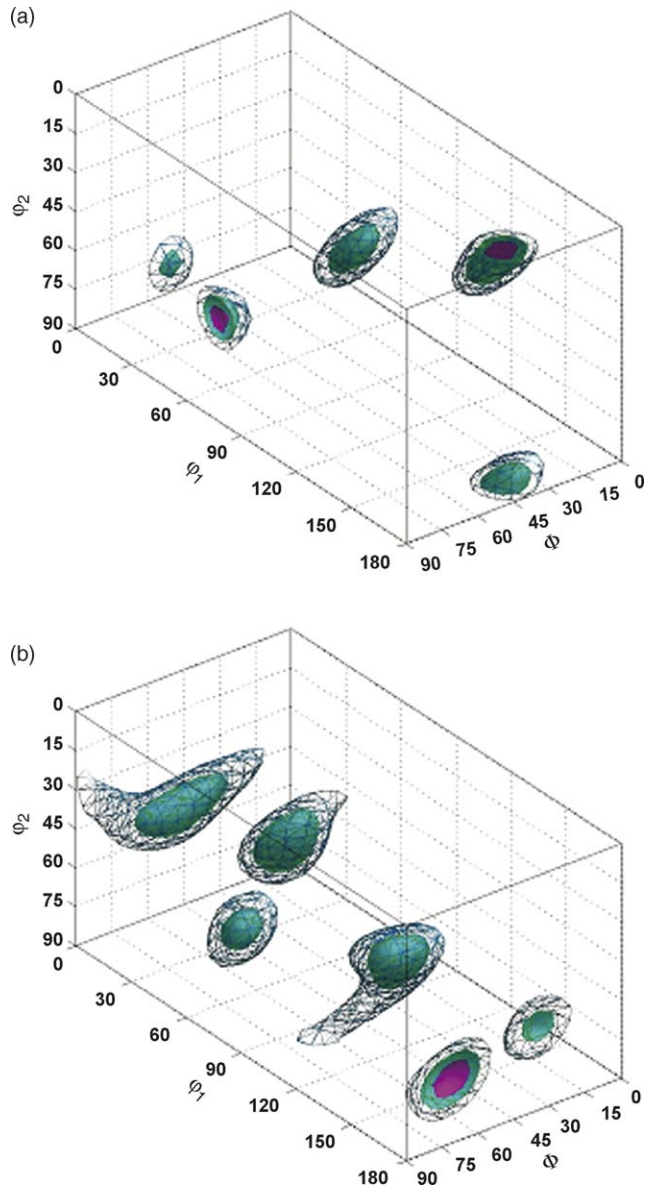


Fig. 6. 3D ODFs for ECAP of aluminum following route $B_C$: (a) 4 passes (maximum intensity is 67.0 × random); (b) 12 passes (maximum intensity is 16.8 × random). Surfaces: 1/4, 1/2 and 3/4 of maximum intensity.

Table 1
Fraction of high-angle boundaries in ECAP aluminum

| | Number of passes | | | | | | |
|---|---|---|---|---|---|---|---|
| | 1 | 4 | | | 12 | | |
| Route | – | A | $B_C$ | C | A | $B_C$ | C |
| Fraction of HAB (%) | ∼10.0 | 30.8 | 22.3 (17.5[a]) | 42.6 | 73.1 | 75.0 (40[a]) | 64.0 |

[a] Number fractions of HAB as measured by TEM/TOCA.

the different processing routes after 4 and 12 passes are within the standard error of measurements [9].

## 4. Discussion

### 4.1. Comparison of the experimental and model textures

Fig. 10(a) shows pole figures for a simple shear calculation by VPSC in the $x'$–$y'$–$z'$ axes of Fig. 1 that corresponds to a strain equivalent to a single idealized ECAP pass through a 90° die in a material with an initially random texture. In this calculation, a negative shear was imposed in the $x'$-direction while $z'$ was taken as the shear plane normal, and the data are shown in Fig. 10(a) relative to the $x$–$y$–$z$-axes of Fig. 1. The VPSC code predicts an essentially uniform distribution of orientations among the A and B shear-texture fibers and the C-orientation. In Fig. 10(b), the calculated texture is shown in a 3D ODF relative to the $x$–$y$–$z$-axis system while points corresponding to individual orientations separated by 5° along the A- and B-fibers, as well as the C-orientation [12], are superimposed on the representation. If the FPN for simple shear is assumed to coincide with the FPN for ECAP, the calculated and experimental shear-texture orientations should coincide in the ODF. The Euler angles using Bunge's definition and the Miller indices for the main shear-texture orientations are given in Table 2. In summary, these data reveal that an ideal shear texture comprises tubes of crystallographically distinct but symmetrically equivalent orientations in the fundamental zone of the ODF. These individual tubes form a connected network in the full Euler space. Fig. 10 and Table 2 show that the A- and B-fibers have common orientations

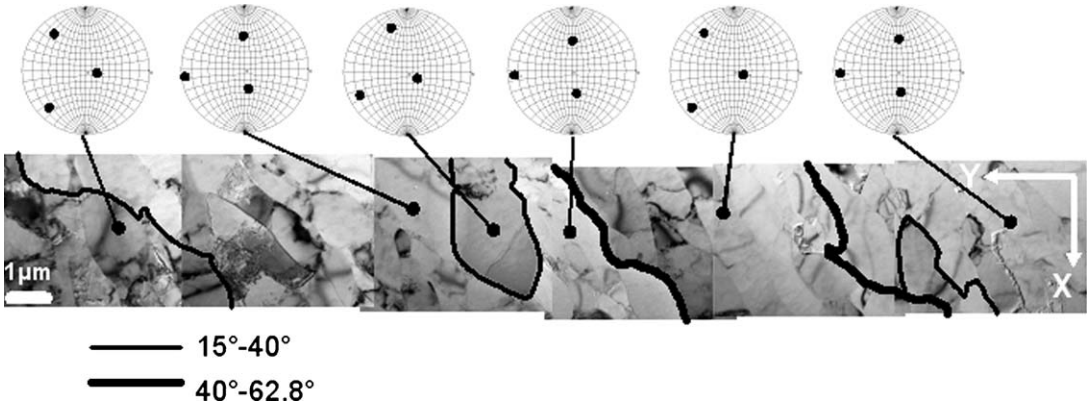


Fig. 7. Bright field TEM images of aluminum processed by four ECAP passes following route $B_C$. Selected grain orientations are shown in the 0 0 2 projections and ranges of boundary disorientations are indicated by the superimposed lines. The DB structure illustrated in the OIM data of Fig. 4 is also apparent here. The coordinate axis system corresponds to the axes in Fig. 1.

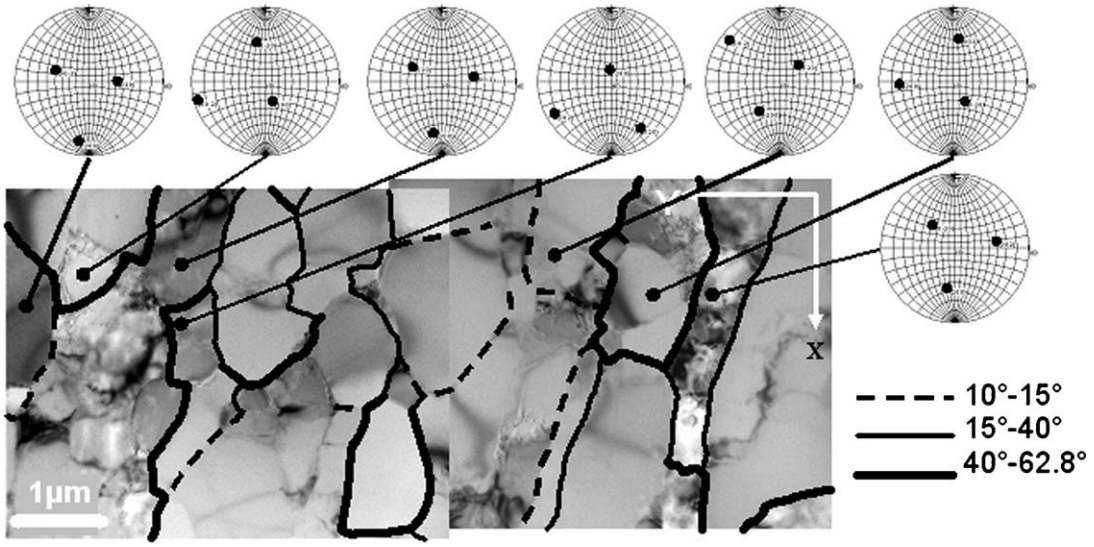


Fig. 8. Bright field TEM images of aluminum processed by 12 ECAP passes following route $B_C$. Selected grain orientations are shown in the 0 0 2 projections and ranges of boundary disorientations are indicated by the superimposed lines. The DB structure is no longer apparent at this resolution after 12 ECAP passes. The coordinate axis system is defined in Fig. 1.

(denoted by B/A in Table 1) and that the C-orientation lies at one end of the B-fiber.

Comparisons of Fig. 10 with the experimental ODF data in Fig. 2 for the initial ECAP pass and in Fig. 6 for material that had been repetitively pressed by route $B_C$ reveals that the experimental textures comprise a few prominent shear-texture orientations that are not uniformly distributed along the A and B orientation fibers. Instead the experimental textures correspond to A- or B-fiber orientations, or to the C-component, and the observed orientations are nearby locations expected for idealized ECAP.

An alternative interpretation of the observed texture components involves a positive shear on the billet $x$–$z$ plane with the SD parallel to the $x$-direction. In a recent discussion of this interpretation [32] the authors distinguished ECAP textures from textures that can be described as a positive simple shear aligned with the die-exit direction in the $x$–$y$ plane. They noted that the difference between an A-fiber component (i.e., $\{1\,1\,1\}\langle 1\,1\,2\rangle$) and a C-orientation (i.e., $\{0\,0\,1\}\langle 1\,1\,0\rangle$) is about 53° and this is close to the angle of rotation about the $z$-axis between a coordinate system corresponding to idealized ECAP and a coordinate system for simple shear in the die-exit direction. In fact, this difference would be indistinguishable for ECAP processing conducted with a die channel angle of 105°. Moreover, a simple analysis of the shape change of a volume element during idealized ECAP and, alternatively, simple shear in the die-exit direction reveal that the shape change is the same in both oper-

Table 2
Some texture orientations of cubic materials for ideal ECAP shear in the fundamental zone of Euler space

| Type of shear components | Shear plane ($x'$–$y'$–$z'$) | | Flow plane ($x$–$y$–$z$) | |
|---|---|---|---|---|
| | Miller indexes, $\{h\,k\,l\}\langle u\,v\,w\rangle$ | Euler angles, $\varphi_1$, $\Phi$, $\varphi_2$ (°) | Miller indexes, $\{h\,k\,l\}\langle u\,v\,w\rangle$ | Euler angles, $\varphi_1$, $\Phi$, $\varphi_2$ (°) |
| A-fiber $\{1\,1\,1\}\langle h\,k\,l\rangle$ | | | | |
| $A_1$ | $(1\,1\,1)[\bar{1}\,\bar{1}\,2]$ | *90*, *54.7*, *45* | $(1\,1\,1)[\overline{11}\,3\,8]$ | *135*, *54.7*, *45* |
| $A_2$ | $(1\,1\,1)[1\,\bar{2}\,2]$ | *30*, *54.7*, *45* | $(1\,1\,1)[3\,8\,\overline{11}]$ | *75*, *54.7*, *45* |
| A/B-intersection | | | | |
| $A/B_1$ | $(1\,1\,1)[1\,0\,\bar{1}]$ | *120*, *54.7*, *45* | $(1\,1\,1)[\overline{11}\,3\,8]$ | *165*, *54.7*, *45* |
| $A/B_2$ | $(1\,1\,1)[0\,\bar{1}\,1]$ | *60*, *54.7*, *45* | $(111)[\bar{8}\,\bar{3}\,1\,1]$ | *105*, *54.7*, *45* |
| B-fiber $\{h\,k\,l\}\langle 1\,1\,0\rangle$ | | | | |
| $B_1$ | $(1\,1\,2)[1\,\bar{1}\,0]$ | *0*, *35.3*, *45* | $(1\,1\,2)[1\,\bar{9}\,4]$ | *45*, *35.3*, *45* |
| | $(1\,2\,1)[\bar{1}\,0\,1]$ | *129.2*, *65.9*, *26.6* | $(1\,2\,1)[\bar{9}\,4\,1]$ | *174.2*, *65.9*, *26.6* |
| $B_2$ | $(2\,1\,1)[0\,\bar{1}\,1]$ | *50.8*, *65.9*, *63.4* | $(2\,1\,1)[4\,1\,\bar{9}]$ | *95.8*, *65.9*, *63.4* |
| C-component $\{1\,0\,0\}\langle 1\,1\,0\rangle$ | | | | |
| C | $(0\,0\,1)[1\,\bar{1}\,0]$ | *45*, *0*, *0* | $(0\,0\,1)[0\,\bar{1}\,0]$ | *90*, *0*, *0* |
| | $(0\,1\,0)[1\,0\,1]$ | *45*, *90*, *0* | $(0\,1\,0)[0\,0\,1]$ | *90*, *90*, *0* |
| | $(1\,0\,0)[1\,\bar{1}\,0]$ | *45*, *90*, *90* | $(0\,0\,1)[\bar{1}\,0\,0]$ | *90*, *90*, *90* |
| | $(0\,0\,1)[\bar{1}\,\bar{1}\,0]$ | *135*, *0*, *0* | $(0\,0\,1)[\bar{1}\,0\,0]$ | *180*, *0*, *0* |
| | $(0\,1\,0)[\bar{1}\,0\,1]$ | *135*, *90*, *0* | $(0\,1\,0)[\bar{1}\,0\,0]$ | *180*, *90*, *0* |
| | $(1\,0\,0)[0\,1\,1]$ | *135*, *90*, *90* | $(0\,0\,1)[0\,1\,0]$ | *180*, *90*, *90* |

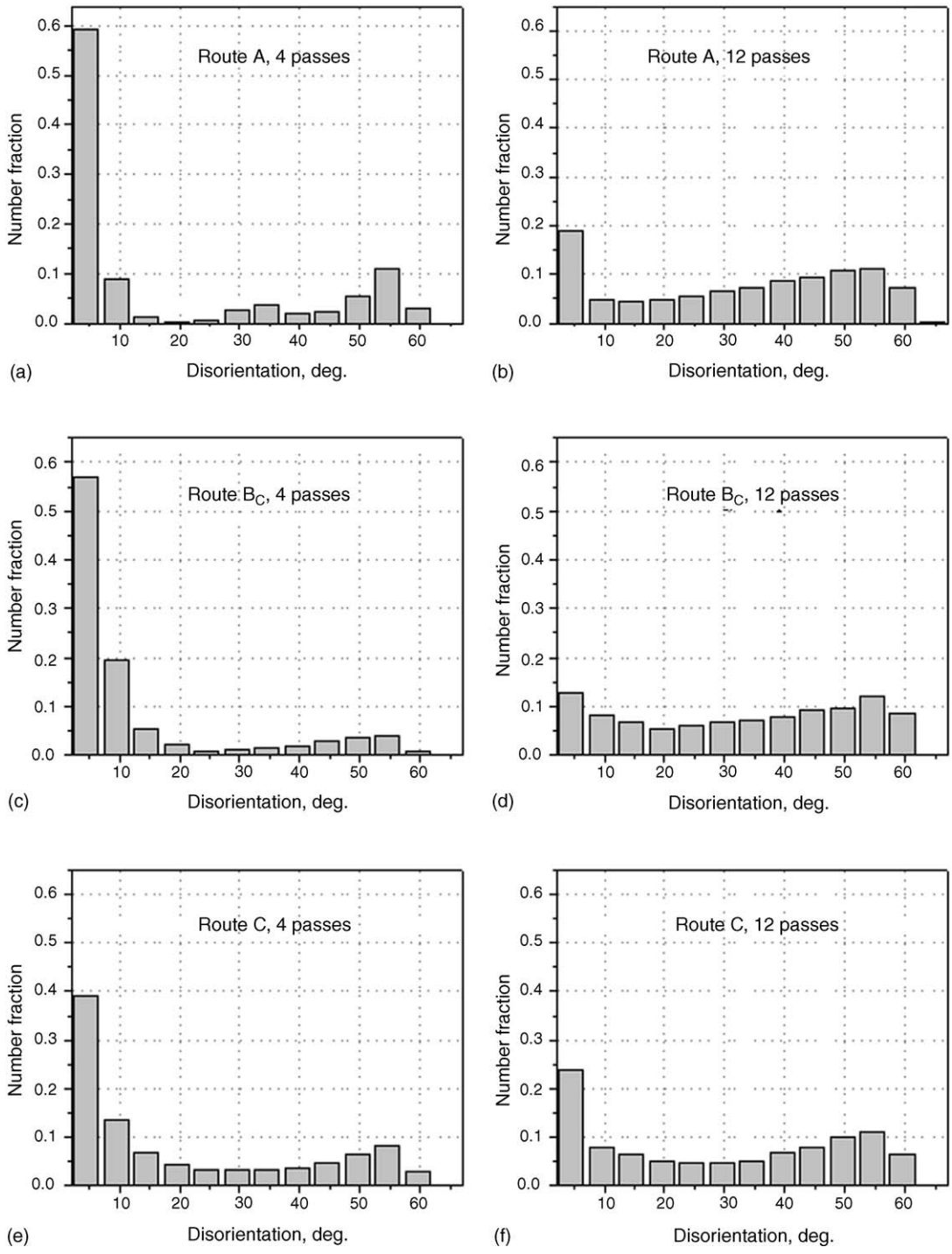


Fig. 9. Grain boundary disorientation distributions in aluminum processed by ECAP: (a) 4 passes by route A; (b) 12 passes by route A; (c) 4 passes by route $B_C$; (d) 12 passes by route $B_C$; (e) 4 passes by route C; (f) 12 passes by route C.

ations if a counterclockwise rotation of 90° about the FPN is introduced before the latter operation. The combination of scatter and the prominence of only certain discrete orientations in experimental texture data precludes unambiguous determination of the location of the shear plane and the shear direction when the data are acquired in the billet axis system. In practice, texture analysis is further complicated by scatter and texture rotations due to frictional and hardening effects.

The A-fiber orientations present after the initial pass in Fig. 2(d) are absent after 4 passes but are apparent again after 12 passes. For the sample processed through four passes by route $B_C$, two distinct orientations are evident in Fig. 6(a) corresponding to A- and B-fiber orientations. For this condition, the lattice orientations within the DBs in Fig. 4(b) alternate between these two shear-texture components. Thus, the shear textures persist throughout repetitive ECAP and the apparent orientations of the

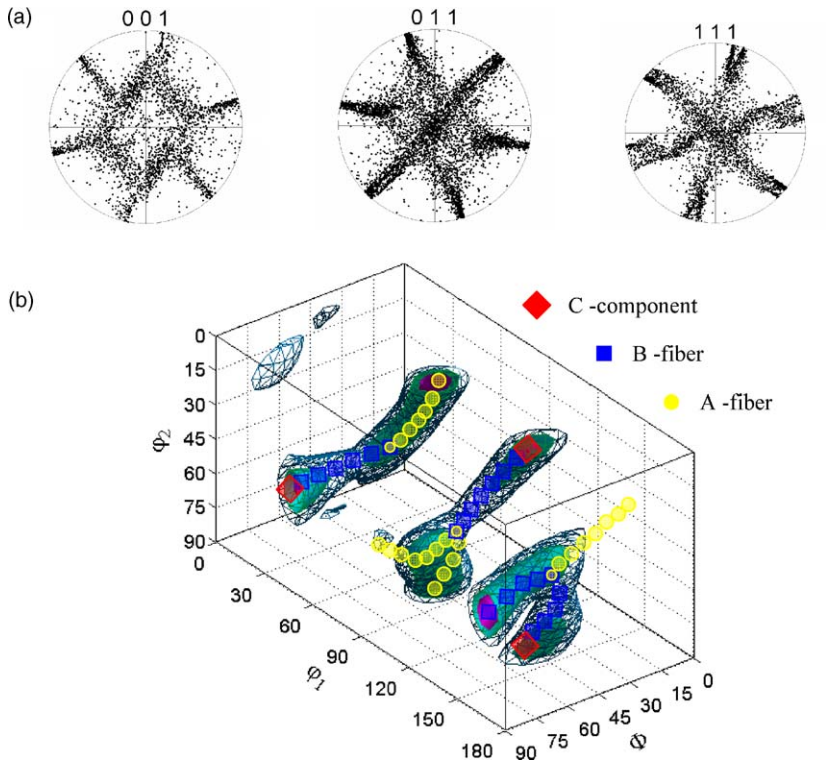


Fig. 10. Pole figures calculated by VPSC from 500 initially random grain orientations that were subjected to one ECAP pass (a), the 3D ODF for these data (b) including discrete orientations along the A- and B-fiber as well as the C-orientation. Low-index shear-texture components are listed in Table 2.

SD and SPN in the texture are established by the final pass in the processing sequence. Furthermore, the orientation of the apparent SD is constant (to within ±4°) throughout the repetitive processing sequences employed in this investigation. Modeling (e.g., [32]) of repetitive ECAP following these various processing routes predicts a persistence of the shear textures but not the appearance of particular orientations and their evolution during a sequence of pressing operations. Furthermore, these modeling procedures do not incorporate processes of grain subdivision such as DB and yet the presence of DBs is clearly a prominent feature in the present data at least after four passes.

### 4.2. Grain refinement and DBs in aluminum processed by ECAP

Predictive models for the micrometer or sub-micrometer grain sizes produced by repetitive ECAP remain to be fully developed. In earlier work on this nominally pure aluminum, TEM images showed that a single ECAP pass at room temperature led to the development of elongated bands of (sub)grains [9]. These (sub)grains were ∼1.2 μm in width, ∼4 μm in length and inclined to bisect the die angle [9,33,34]. A banded microstructure was also evident in OIM results except only that the bands were non-uniform in size throughout the sample [9].

In the present investigation, the OIM results show that the microtextures are highly inhomogeneous and there is a long-range curvature of the lattice within the subgrain structure (Figs. 2 and 3). While local microtextures vary from location to location, the observed orientations are always part of a macroscopic shear texture in the sample. Alternating bands of orientations are not apparent after one ECAP pass although there are high-angle boundaries separating different texture orientations. The initial grain size of this material was large (∼1 mm) and the associated texture was predominantly random so that most of these boundaries reflect processes of grain subdivision during the initial ECAP pass.

Pure aluminum pressed four times by routes A and $B_C$ exhibits essentially the same microtextures and DBs having orientations corresponding to two distinct orientations in the texture. These DB-like features are also apparent in material processed by route C although more than two orientations are generally found in all regions examined. The interfaces between the DBs are inclined at an angle of about 26° to the axis of the die exit channel and this corresponds closely to the angle between the edges of a cubic volume element after passage through the die. Thus, in Fig. 1 the line segments $\overline{1'2'}$ and $\overline{3'4'}$ are inclined at an angle of 26.6° to $\overline{1'4'}$ and $\overline{2'3'}$, respectively. The bands vary in thickness from ∼5 to 25 μm and therefore they have developed within the prior grains. The present results are consistent with the current understanding of DB. The two orientations apparent in material processed by routes A and $B_C$ are a C-type orientation and an A/B-type orientation.

The TEM data demonstrate the presence of subgrains having a size of ∼1.2 μm within the DBs in material processed through four passes by route $B_C$. Furthermore, a collection of CBED data over a large area in thin foils confirmed the presence of alternating bands of (sub)grains separated by high-angle boundaries, as shown in Fig. 7. A detailed analysis of the boundary struc-

ture was not part of this research but nevertheless it is apparent that the boundaries are distinct and well-defined and they do not appear as transition bands or local regions containing a fine subgrain structure. The alternating orientations obtained in the TEM data may be attributed to various components of the shear texture although the orientations differ somewhat from those seen in the OIM analysis.

Repetitive pressing of the pure aluminum through 12 ECAP passes leads to a break-up of the distinct DB structure that was apparent after 4 passes. Instead, as illustrated in Fig. 8, the microstructure consists of (sub)grain clusters that each appear to belong to a shear-texture component. Nevertheless, careful examination of the microstructures in Figs. 5 and 8 reveals a long-range alignment of these clusters suggesting there is a remnant of the band structure that was apparent after four ECAP passes. Disorientation distributions reported in a previous study of this pure aluminum [31] indicated a relative increase in the population of high-angle boundaries after 12 ECAP passes. Such an increase in high-angle boundaries is evident in a comparison of the point-to-origin traverses for route $B_C$ in Figs. 4(a) and 5(a) and also in a comparison of the TEM data in Figs. 7 and 8. Nevertheless, a significant fraction of low-angle boundaries remains after 12 passes and the disorientations of the high-angle boundaries correspond to the disorientations between deformation-induced shear-texture components. Thus, this represents a deformation-induced microstructure.

### 4.3. Development of a model for microstructural evolution

The evolution of microstructure during ECAP processing of aluminum involves primarily grain deformation and substructure formation in the initial pass which is then followed by the development of a distinct DB structure after four passes. The formation of DBs permits a minimization of the energy expenditure during deformation because these regions are oriented to minimize the number of active slip systems and hence to reduce the probability of dislocation entanglement and pinning. An alternating arrangement of DBs accommodated by substructure formation within the bands is then necessary to accommodate the macroscopic shape change. In addition, the interfaces between the DBs are high-angle in nature and this accounts, at least in part, for the increase in the fraction of high-angle boundaries after pressing through four passes.

A mechanism describing the build-up in the proportion of high-angle boundaries during ECAP must necessarily involve the repeated subdivision of the microstructure by DB formation combined with an evolution in the DBs through a sequence of repetitive pressing operations. The elongation and thinning, band–band intersections and internal subdivision through a sequence of ECAP passes will accordingly increase the total area of the DB interfaces and may result also in a fragmentation of the band structure. The continued presence of low-angle boundaries reflects the formation of a subgrain structure within the DBs.

Following an earlier approach [19], the scale of the substructure is dictated by the Zener–Hollomon parameter, $Z = \dot{\varepsilon} \exp(Q/RT)$, where $\dot{\varepsilon}$ is the strain rate during an ECAP pass, $Q$ the activation energy for deformation, $R$ the gas constant and $T$ is the pressing temperature. Here, the material composition and pressing speed and temperature are nearly identical to those of the earlier investigation, wherein a value of $\ln Z = 65.4$ corresponded to a grain size of ~1.3 μm. The grain size was only weakly dependent on strain rate and temperature for large strain deformation at temperatures near ambient [19], and, thus, a (sub)grain size of ~1.2 μm in the TEM data of Figs. 7 and 8 is consistent with an approximately constant substructure scale through a sequence of pressing passes. By contrast, the process of DB evolution during repetitive ECAP leads to a decreased volume and increased interfacial area for each individual band or band fragment. The sub-boundaries will interact with high-angle DB interfaces and result in serration of these interfaces; such serration of the high-angle boundaries is evident in the TEM image of Fig. 7. At a critical strain, one or more of the DB dimensions will be reduced to the substructure size. At this point, capillarity effects will lead to a pinching-off of the individual subgrains and the formation of an equiaxed structure having low-angle boundaries but with a large proportion of high-angle boundaries [35], and the TEM data of Fig. 8 are consistent with such an effect. Close inspection shows that this mechanism has similarities to the geometric dynamic recrystallization model proposed initially to describe grain refinement in aluminum alloys during warm-rolling [21] except only that the rolling model incorporates the elongation of individual grains instead of the DBs that are an inherent feature of the microstructure after ECAP.

There has been extensive recent discussion concerning the fraction of high-angle boundaries and the effectiveness of the different ECAP processing routes [36–40]. Direct measurements on pure metals using automated EBSD have shown there often remains a high fraction of LAB after ECAP [40]. By contrast, ECAP of nickel gave a high population (~70%) of HABs after eight passes when using route $B_C$ [36]. The suggestion from Fig. 9 and Table 1 is that a fractional value of HABs of about 70% is close to the saturation limit for pure Al after 12 passes.

## 5. Conclusions

(1) Processing by ECAP of nominally pure aluminum leads to the development of an inhomogeneous shear texture after an initial pass. Repetitive ECAP pressing up to 12 passes produces a homogenization of the texture. The main components of the texture are always shear components.
(2) From an analysis of the texture data, it is concluded that the shear plane and shear direction correspond to the idealized ECAP model with a deviation of 10° which is attributed to the influence of the die-relief angle, strain hardening during deformation and to frictional effect at the die walls.
(3) An OIM analysis of all processing routes and a TEM/TOCA investigation of route $B_C$ confirm that alternating bands of distinct orientations are formed in the processing of pure aluminum by ECAP. These deformation bands became especially pronounced after 4 passes of ECAP and there is further refinement of the microstructure after processing through 12 passes.

(4) A mechanism is proposed for microstructural evolution involving the formation of deformation bands, their evolution and interaction with the accompanying subgrain structure, and the increasing population of high-angle boundaries that are present after repetitive ECAP. In this investigation, a high fraction of high-angle boundaries is achieved after 12 passes of ECAP irrespective of the processing route.

## Acknowledgements

One of the authors (A.P.Z.) thanks the National Research Council of the National Academy of Science (U.S.A.) for financial support. Another author (T.G.L.) was supported by the U.S. Army Research Office under Grant No. W911NF-05-1-0046, while TRM was partially supported by the U.S. Air Force Office of Scientific Research under Grant. No. F1ATA06058G001. The work was also partially supported by INTAS-03513779 and RFBR-05-03-32233-a.

## References

[1] Z. Horita, M. Furukawa, M. Nemoto, A.J. Barnes, T.G. Langdon, Acta Mater. 48 (2000) 3633.
[2] S. Komura, P.B. Berbon, M. Furukawa, Z. Horita, M. Nemoto, T.G. Langdon, Scr. Mater. 38 (1998) 1851.
[3] N.A. Akhmadeev, V.I. Kopylov, R.R. Mulyukov, R.Z. Valiev, Russ. Metal. 5 (1992) 96.
[4] J. Wang, Z. Horita, M. Furukawa, M. Nemoto, N.K. Tsenev, R.Z. Valiev, Y. Ma, T.G. Langdon, J. Mater. Res. 8 (1993) 2810.
[5] T.G. Langdon, M. Furukawa, M. Nemoto, Z. Horita, JOM 52 (4) (2000) 30.
[6] A.P. Zhilyaev, G.V. Nurislamova, B.-K. Kim, M.D. Baró, J.A. Szpunar, T.G. Langdon, Acta Mater. 51 (2003) 753.
[7] S. Komura, Z. Horita, M. Nemoto, T.G. Langdon, J. Mater. Res. 14 (1999) 4044.
[8] H. Miyamoto, U. Erb, T. Koyama, T. Mimaki, A. Vinogradov, S. Hashimoto, Philos. Magn. Lett. 84 (2004) 235.
[9] S.D. Terhune, D.L. Swisher, K. Oh-ishi, Z. Horita, T.G. Langdon, T.R. McNelley, Metall. Trans. A 33A (2002) 2173.
[10] Q. Jining, J. Han, Z. Guoding, J. Lee, Scr. Mater. 51 (2004) 185.
[11] G.R. Canova, U.F. Kocks, J.J. Jonas, Acta Metall. 32 (1984) 211.
[12] F. Montheillet, M. Cohen, J.J. Jonas, Acta Metall. 32 (1984) 2077.
[13] Y. Fukuda, K. Oh-ishi, M. Furukawa, Z. Horita, T.G. Langdon, Acta Mater. 52 (2004) 1387.
[14] S. Ferrasse, V.M. Segal, S.R. Kalidindi, F. Alfrod, Mater. Sci. Eng. A 368 (2004) 28.
[15] S. Ferrasse, V.M. Segal, F. Alfrod, Mater. Sci. Eng. A 372 (2004) 235.
[16] I.J. Beyerlein, R.A. Lebensohn, C.N. Tomé, Mater. Sci. Eng. A 345 (2003) 122.
[17] L.S. Tóth, R.A. Massion, L. Germain, S.C. Baik, S. Suwas, Acta Mater. 52 (2004) 1885.
[18] A. Gholinia, P. Bate, P.B. Prangnell, Acta Mater. 50 (2002) 2121.
[19] S.L. Semiatin, P.B. Berbon, T.G. Langdon, Scr. Mater. 44 (2001) 135.
[20] P.B. Prangnell, R.J. Bowen, in: Y.T. Zhu, T.G. Langdon, R.S. Mishra, S.L. Semiatin, M.J. Saran, T.C. Lowe (Eds.), Ultrafine Grained Materials, vol. II, TMS, Warrendale, PA, 2002, pp. 89–98.
[21] A. Gholinia, F.J. Humphreys, P.B. Prangnell, Acta Mater. 50 (2002) 4461.
[22] D. Kuhlmann-Wilsdorf, Metall Mater. Trans. A 35A (2004) 388.
[23] T.R. McNelley, D.L. Swisher, M.T. Pérez-Prado, Metal. Mater. Trans. A: 33A (2002) 279.
[24] M.T. Pérez-Prado, T.R. McNelley, D.L. Swisher, G. González-Doncel, O. Ruano, Mater. Sci. Eng. A 342 (2003) 216.
[25] D.A. Hughes, N. Hansen, Acta Mater. 45 (1997) 3871.
[26] D.A. Hughes, N. Hansen, Acta Mater. 48 (2000) 2985.
[27] S.C. Vogel, D.J. Alexander, I.J. Beyerlein, M.A.M. Bourke, D.W. Brown, B. Clausen, C.N. Tomé, R.B. Von Dreele, C. Xu, T.G. Langdon, Mater. Sci. Forum 426–432 (2003) 2661.
[28] C. Xu, T.G. Langdon, Scr. Mater. 48 (2003) 1.
[29] V. Randle, O. Engler, Introduction to Texture Analysis: Macrotexture, Microtexture and Orientation Mapping, Taylor & Francis, London, 2002, p. 388.
[30] R.A. Lebensohn, C.N. Tomé, Acta Mater. 41 (1993) 2611.
[31] T.R. McNelley, D.L. Swisher, Z. Horita, T.G. Langdon, in: Y.T. Zhu, T.G. Langdon, R.Z. Valiev, S.L. Semiatin, D.H. Shin, T.C. Lowe (Eds.), Ultrafine Grained Materials, vol. III, TMS, Warrendale, PA, 2004, p. 89.
[32] S. Li, I.J. Beyerlein, M.A.M. Bourke, Mater. Sci. Eng. A 394 (2005) 66.
[33] Y. Iwahashi, Z. Horita, M. Nemoto, T.G. Langdon, Acta Mater. 45 (1997) 4733.
[34] Y. Iwahashi, Z. Horita, M. Nemoto, T.G. Langdon, Acta Mater. 46 (1998) 3317.
[35] T.R. McNelley, D.L. Swisher, Mater. Sci. Forum. 447–448 (2004) 373.
[36] A.P. Zhilyaev, B.-K. Kim, G.V. Nurislamova, M.D. Baró, J.A. Szpunar, T.G. Langdon, Scr. Mater. 46 (2002) 575.
[37] A. Gholinia, P.B. Prangnell, M.V. Markushev, Acta Mater. 48 (2000) 1115.
[38] J.R. Bowen, O.V. Mishin, P.B. Prangnell, D. Juul Jensen, Scr. Mater. 35 (1996) 873.
[39] G. Wang, S.D. Wu, L. Zuo, C. Esling, Z.G. Wang, G.Y. Li, Mater. Sci. Eng. A 346 (2003) 83.
[40] O.V. Mishin, D. Juul Jensen, N. Hansen, Mater. Sci. Eng. A 342 (2003) 320.